

ARTICLE

Received 14 Apr 2016 | Accepted 16 Aug 2016 | Published 28 Sep 2016

DOI: 10.1038/ncomms12921

OPEN

# Return of naturally sourced Pb to Atlantic surface waters

Luke Bridgestock<sup>1,†</sup>, Tina van de Flierdt<sup>1</sup>, Mark Rehkämper<sup>1</sup>, Maxence Paul<sup>1</sup>, Rob Middag<sup>2,3</sup>, Angela Milne<sup>4</sup>, Maeve C. Lohan<sup>5</sup>, Alex R. Baker<sup>6</sup>, Rosie Chance<sup>6,†</sup>, Roulin Khondoker<sup>1</sup>, Stanislav Strekopytov<sup>7</sup>, Emma Humphreys-Williams<sup>7</sup>, Eric P. Achterberg<sup>8</sup>, Micha J.A. Rijkenberg<sup>9</sup>, Loes J.A. Gerringa<sup>9</sup> & Hein J.W. de Baar<sup>9</sup>

Anthropogenic emissions completely overwhelmed natural marine lead (Pb) sources during the past century, predominantly due to leaded petrol usage. Here, based on Pb isotope measurements, we reassess the importance of natural and anthropogenic Pb sources to the tropical North Atlantic following the nearly complete global cessation of leaded petrol use. Significant proportions of up to 30–50% of natural Pb, derived from mineral dust, are observed in Atlantic surface waters, reflecting the success of the global effort to reduce anthropogenic Pb emissions. The observation of mineral dust derived Pb in surface waters is governed by the elevated atmospheric mineral dust concentration of the North African dust plume and the dominance of dry deposition for the atmospheric aerosol flux to surface waters. Given these specific regional conditions, emissions from anthropogenic activities will remain the dominant global marine Pb source, even in the absence of leaded petrol combustion.

<sup>1</sup>Department of Earth Science and Engineering, Imperial College London, London SW7 2AZ, UK. <sup>2</sup>Department of Chemistry, NIWA/University of Otago Research Centre for Oceanography, Dunedin 9054, New Zealand. <sup>3</sup>Department of Ocean Sciences & Institute of Marine Sciences, University of California Santa Cruz, CA 95064, USA. <sup>4</sup>School of Geography, Earth and Environmental Sciences, University of Plymouth, Plymouth PL4 8AA, UK. <sup>5</sup>Ocean and Earth Sciences, National Oceanography Centre Southampton, University of Southampton, Southampton SO14 3ZH, UK. <sup>6</sup>School of Environmental Sciences, University of East Anglia, Norwich NR4 7TJ, UK. <sup>7</sup>Image and Analysis Centre, Natural History Museum, London SW7 5BD, UK. <sup>8</sup>Geomar-Helmholtz Centre for Ocean Research, Kiel 24148, Germany. <sup>9</sup>Department of Ocean Systems (OCS), NIOZ Royal Netherlands Institute for Sea Research, and Utrecht University, P.O. Box 59, 1790 AB Den Burg, Texel, The Netherlands. † Present addresses: Department of Earth Sciences, University of Oxford, Oxford OX1 3AN, UK (L.B.); Wolfson Atmospheric Chemistry Laboratory, Department of Chemistry, University of York, York YO10 5DD, UK (R.C.). Correspondence and requests for materials should be addressed to L.B. (email: luke.bridgestock@earth.ox.ac.uk).

Anthropogenic activities have significantly perturbed the global biogeochemical cycles of numerous trace metals<sup>1</sup>. One of the most extensively perturbed and documented biogeochemical cycles is that of lead (Pb; refs 2,3). The combustion of leaded petrol constitutes the dominant environmental Pb source during the past century, along with emissions from non-ferrous metal smelting, coal combustion and waste incineration<sup>1,4</sup>. The ocean has been strongly affected by this perturbation with even the deepest waters dominated by anthropogenic Pb (ref. 2). Historically, the North Atlantic received the highest anthropogenic Pb inputs due to its proximity to the industrialized regions of North America and Europe<sup>5–7</sup>. On the basis of coral records from Bermuda, the onset of the anthropogenic Pb perturbation of North Atlantic surface waters extends back to ~1850 (ref. 7). Previous studies of Atlantic seawater sampled since the late 1970s, found furthermore that anthropogenic sources completely dominated modern marine Pb inventories<sup>5–12</sup>. The short residence time of Pb in ocean surface waters (several years), means their Pb content closely tracks atmospheric inputs<sup>5,6,13,14</sup>. For example, Pb concentrations in North Atlantic surface waters rose from pre-anthropogenic values of ~15 pmol kg<sup>-1</sup> to a peak of ~200 pmol kg<sup>-1</sup> in the 1970s, before sharply declining (by a factor of ~5) during the 1980s and 1990s, a trend that largely reflects the increased usage and subsequent phasing-out of leaded petrol in the surrounding regions<sup>6,7</sup>.

Surface waters of the tropical North Atlantic (0–30°N) receive the largest inputs of mineral dust in the entire global ocean via the North African dust plume<sup>15</sup>, which represents a potentially important natural source of Pb. However, studies conducted in the 1980s and 1990s found Pb in surface waters of this region to be dominated by anthropogenic sources, despite dramatically decreasing anthropogenic inputs at that time<sup>8–10</sup>. Almost complete cessation of global leaded petrol use has since been achieved, with North African countries among the last to phase-out following the Dakar Declaration in 2002 (ref. 16). With the termination of this prominent anthropogenic Pb flux, natural sources may once again provide significant contributions to Pb budgets of tropical North Atlantic surface waters.

The detection of significant amounts of natural Pb in ocean surface waters would not only be a testament to the global effort to reduce anthropogenic Pb emissions, but would also provide an unprecedented opportunity to study the factors governing marine Pb inputs from both anthropogenic and natural sources. In

particular, the relative proportions of Pb derived from mineral dust and anthropogenic emissions in ocean surface waters will be influenced by the relative atmospheric concentrations, deposition velocities and solubilities in seawater from aerosols of these two Pb sources. Such factors, typically highly variable in space and time, will be integrated over the residence time of Pb in ocean surface waters.

Mineral dust emitted in North Africa is transported across the tropical North Atlantic year round, albeit with considerable seasonal variability. Notably, the main focus of mineral dust transport moves northward, from around 4°N to 20°N between the boreal winter and boreal summer, following the seasonal migration of the inter tropical convergence zone (ITCZ)<sup>17</sup>. This latitudinal shift has a pronounced effect on the delivery of mineral dust to sites in the western tropical North Atlantic (WTA)<sup>18</sup>. The altitude at which mineral dust is transported over the tropical North Atlantic also varies seasonally, with low-level transport in the marine boundary layer during the boreal winter and transport in the Saharan air layer at altitudes of about 1–7 km during the boreal summer<sup>19–21</sup>. Consequently, mineral dust deposition rates in the eastern tropical North Atlantic (ETA) are higher in winter than in summer months<sup>20,22</sup>.

Here we reassess the importance of natural Pb sources to tropical North Atlantic surface waters, following the almost complete global phase-out of leaded petrol, and study the factors governing the relative atmospheric fluxes of anthropogenic and mineral dust derived Pb to surface waters of this region. We thereby present and interpret Pb concentration and isotope composition data for surface seawater samples, collected during the second leg cruise of the GEOTRACES section GA02 (64PE321; June–July, 2010) and the GEOTRACES section GA06 (D361; February–March, 2011) in the WTA and ETA respectively, in addition to atmospheric aerosols collected in the ETA during the GA06 section. These two quasi-meridional cruise transects were conducted at different times of the year, hence they intersect the North African dust plume at different stages of its seasonal migration (Fig. 1). We find that North African mineral dust constitutes a significant source of Pb to surface waters of this region, accounting for up to 30–50% of the total Pb budgets. Furthermore, we demonstrate that more efficient deposition of mineral dust relative to anthropogenic particles by dry deposition plays a key role in producing the observed proportions of these two Pb sources in ocean surface waters.

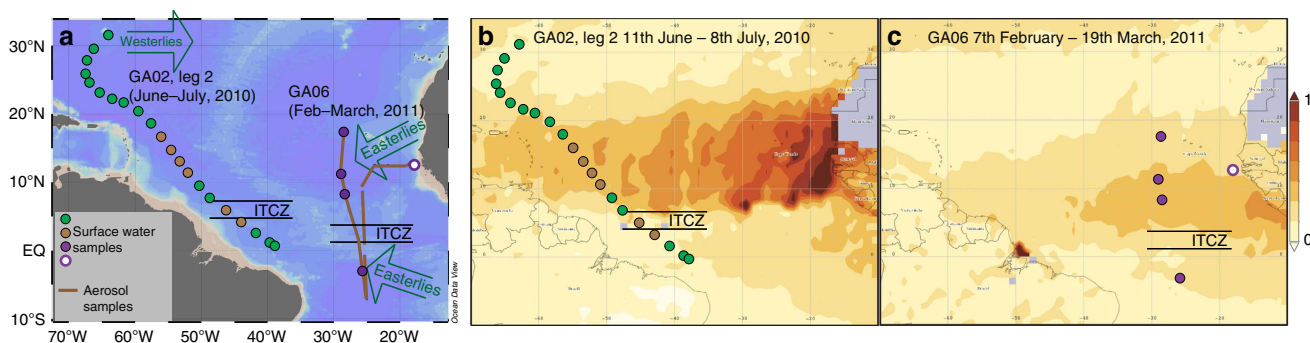


**Figure 1 | Collection locations of samples used in this study.** Panel (a), sampling locations for unfiltered surface seawater (circles) and aerosols (brown lines) along the middle part of the GEOTRACES section GA02 (2nd leg; cruise PE321) and along the GEOTRACES section GA06 (cruise D361). Brown circles indicate surface seawaters affected by mixing with Amazon River outflow in the western tropical Atlantic (WTA). Green arrows show the main meteorological regimes, while black lines denote the position of the ITCZ (Inter Tropical Convergence Zone) during each cruise. The map was produced using Ocean Data View<sup>69</sup>. Panels (b) and (c) show aerosol optical depth (550 nm) averaged over the duration of the cruises PE321 (section GA02, 2nd leg) and cruise D361 (section GA06) respectively. The position of the North African mineral dust plume over the Atlantic Ocean can be clearly identified by higher values (darker colours). Visualizations were produced using the Giovanni online data system, NASA GES DISC<sup>70</sup> with data from the MODIS instrument on board the Terra satellite.

## Results

**Sources of Pb to ocean surface waters.** Lead isotope ratio measurements can be used to distinguish between different sources of Pb to the ocean (for example, see refs <sup>2,8–12</sup>). Unfiltered surface seawater samples were analysed for total Pb concentrations and isotope compositions (Table 1, Fig. 2a–c; see the ‘Methods’ section). To assess particulate Pb contributions to the samples, total Pb concentrations were compared with data for either filtered (<0.2 μm) or particulate samples (>0.45 μm) collected during the same cruises (Fig. 2a, Supplementary Table 1). It should be noted, that unfiltered samples were collected at slightly different locations and depths to filtered and particulate samples.

The major potential Pb sources to the study regions are, anthropogenic Pb transported by easterly winds originating from Africa and/or Europe<sup>23–25</sup>, anthropogenic Pb transported by westerly winds originating from North and Central America<sup>11,23</sup>, North African mineral dust transported by easterly winds<sup>26–28</sup> and riverine inputs from the Amazon basin<sup>29,30</sup>. These different Pb sources can be distinguished using a plot of <sup>206</sup>Pb/<sup>207</sup>Pb versus <sup>208</sup>Pb/<sup>207</sup>Pb (Fig. 3). In detail, the anthropogenic sources feature low <sup>206</sup>Pb/<sup>207</sup>Pb, <sup>208</sup>Pb/<sup>207</sup>Pb ratios (easterlies) or intermediate <sup>206</sup>Pb/<sup>207</sup>Pb coupled with low <sup>208</sup>Pb/<sup>207</sup>Pb ratios (westerlies), while natural sources (mineral dust and Amazon inputs) feature high <sup>206</sup>Pb/<sup>207</sup>Pb and <sup>208</sup>Pb/<sup>207</sup>Pb ratios. A compilation of the

relevant literature data used to assess the isotope composition of these sources is provided in Supplementary Tables 2–5, with details of these data sets provided in Supplementary Note 1.

In context of these endmembers, surface waters from close to the equator, with low <sup>206</sup>Pb/<sup>207</sup>Pb, <sup>208</sup>Pb/<sup>207</sup>Pb ratios (Fig. 2b,c), contain the highest proportions of anthropogenic Pb transported by easterly winds (Fig. 3). Furthermore, advection of water from the South Atlantic by the North Brazil Current may also contribute to the low <sup>206</sup>Pb/<sup>207</sup>Pb, <sup>208</sup>Pb/<sup>207</sup>Pb ratios of these samples. Concurrent increases in both of these ratios with increasing latitude in the WTA and ETA (Fig. 2b,c) correspond to deviations towards the isotope composition of natural Pb from mineral dust and/or Amazon River inputs (Fig. 3). Maximum values for these ratios occur at 13.2–18.7°N in the WTA and 11.9°N in the ETA, indicating maxima in Pb contributions from natural relative to anthropogenic sources. A less pronounced maximum for these Pb isotope ratios occurs at about 5°N in the WTA. Between ~20 to 30°N in the WTA, <sup>206</sup>Pb/<sup>207</sup>Pb ratios remain high, while <sup>208</sup>Pb/<sup>207</sup>Pb decreases (Fig. 2b,c), corresponding to an increase in the contributions of North/Central American anthropogenic Pb transported by westerly winds (Fig. 3). Between 11.9°N and 17.4°N in the ETA, a concurrent decrease in <sup>206</sup>Pb/<sup>207</sup>Pb and <sup>208</sup>Pb/<sup>207</sup>Pb ratios (Fig. 2b,c) signifies an increasing contribution of anthropogenic Pb transported by easterly winds (Fig. 3).

**Table 1 | Lead concentration and isotope data for unfiltered surface seawater samples collected during along the GEOTRACES sections GA02 (2nd leg) and GA06.**

Sample ID	Latitude (°N)	Longitude (°W)	Date	Pb concentration (pmol kg <sup>-1</sup> )	n <sup>†</sup>	<sup>206</sup> Pb/ <sup>204</sup> Pb	2s.e. <sup>†</sup> (p.p.m.)	<sup>206</sup> Pb/ <sup>207</sup> Pb	2s.e. <sup>†</sup> (p.p.m.)	<sup>208</sup> Pb/ <sup>207</sup> Pb	2s.e. <sup>†</sup> (p.p.m.)	Measured Pb quantity (ng) <sup>‡</sup>
GEOTRACES section GA02; Leg 2; cruise PE321 (western tropical Atlantic) 11th June–8th July, 2010												
Fish 13a	31.70	64.24	13/06	21.51	1	18.4093	150	1.1769	27	2.4468	21	6.0
Fish 13b	29.70	66.44	14/06	22.49	1	18.4034	368	1.1759	43	2.4496	35	3.4
Fish 14	28.04	67.51	16/06	22.28	1	18.4126	288	1.1768	30	2.4513	25	4.2
Fish 16a	26.06	67.72	16/06	24.24	2	18.4187	265	1.1776	32	2.4533	30	5.3
Fish 16b	24.75	67.10	17/06	23.32	1	18.4230	245	1.1769	32	2.4528	30	5.1
Fish 17	23.30	65.58	18/06	22.12	2	18.4650	205	1.1801	35	2.4555	32	4.6
Fish 18	22.38	63.67	19/06	23.20	1	18.4435	178	1.1787	23	2.4538	23	4.7
Fish 19	21.79	61.89	20/06	21.87	3	18.4345	267	1.1779	38	2.4540	35	2.3
Fish 20	20.56	59.72	21/06	23.03	1	18.4231	208	1.1770	30	2.4552	28	4.7
Fish 21	18.74	57.77	22/06	19.12	2	18.4555	241	1.1788	32	2.4570	25	4.8
Fish 22 <sup>  </sup>	16.77	56.22	24/06	16.88	2	18.4383	541	1.1783	62	2.4573	50	1.6
Fish 23 <sup>  </sup>	14.80	54.74	25/06	16.84	2	18.4529	267	1.1779	46	2.4572	37	4.0
Fish 24 <sup>  </sup>	13.15	53.41	26/06	15.00	2	18.4112	459	1.1770	50	2.4561	49	3.3
Fish 25 <sup>  </sup>	11.52	52.15	27/06	17.34	2	18.3623	181	1.1733	31	2.4524	24	4.3
Fish 26	9.50	50.43	28/06	19.78	2	18.3015	238	1.1701	31	2.4488	26	3.6
Fish 27	7.73	48.84	30/06	20.80	2	18.3240	271	1.1712	36	2.4502	29	4.7
Fish 28 <sup>  </sup>	5.93	46.36	01/07	17.73	2	18.3450	206	1.1724	33	2.4513	26	4.6
Fish 29 <sup>  </sup>	4.19	44.04	02/07	18.14	2	18.3336	314	1.1716	37	2.4493	29	3.5
Fish 30	2.62	41.81	03/07	19.19	2	18.2810	311	1.1695	40	2.4472	34	4.0
Fish 31	1.19	39.74	04/07	19.57	2	18.2710	253	1.1679	36	2.4455	27	5.1
Fish 32	0.70	38.97	05/07	23.88	2	18.2584	279	1.1677	34	2.4456	25	4.2
GEOTRACES section GA06; cruise D361 (eastern tropical Atlantic) 7th February–19th March, 2011												
Fish 43 <sup>C,§</sup>	12.59	17.65	22/02	11.52	1	18.3803	289	1.1744	37	2.4567	36	2.0
Fish164	-3.31	25.49	05/03	20.31	1	18.2188	192	1.1651	29	2.4429	21	5.2
Fish 200	8.28	28.31	10/03	15.84	1	18.2834	198	1.1689	31	2.4468	25	4.4
Fish 211	11.90	28.98	11/03	18.78	1	18.3767	274	1.1743	37	2.4508	26	3.2
Fish 227 <sup>§</sup>	17.37	28.39	14/03	16.46	1	18.2843	826	1.1691	102	2.4473	79	3.6

<sup>C</sup>Sample collected off the coast of east Africa.

<sup>n</sup>number of Pb concentration analyses conducted; quoted Pb concentrations are the mean of all analyses, and are corrected for an average blank of 11.7 ± 4.3 pg (1 s.d., n = 36)<sup>66</sup>.

<sup>†</sup>relative within-run precision (2 s.e.) of isotopic data in parts per million (ppm).

<sup>‡</sup>Quantity of Pb utilized for the isotopic analysis.

<sup>§</sup>Pb isotope ratios are assigned a larger level of uncertainty due to either the small quantity of Pb available for analysis (≤2 ng) and/or poor within-run precision. For these samples, <sup>206</sup>Pb/<sup>204</sup>Pb, <sup>206</sup>Pb/<sup>207</sup>Pb and <sup>208</sup>Pb/<sup>207</sup>Pb are assigned relative uncertainties of 2.6%, 1.7% and 0.8% respectively; for all other samples, these isotope ratios are assigned uncertainties of 1%, 1% and 0.25% respectively. The quoted uncertainties are based on replicate analyses (2 s.d.) of in-house seawater reference materials<sup>66</sup>. Similarly, the Pb concentrations are assigned an uncertainty of ±1 pmol kg<sup>-1</sup> based on replicate analyses (1 s.d.) of in-house seawater reference materials<sup>66</sup>.

<sup>||</sup>Samples affected by mixing with Amazon River outflow water.

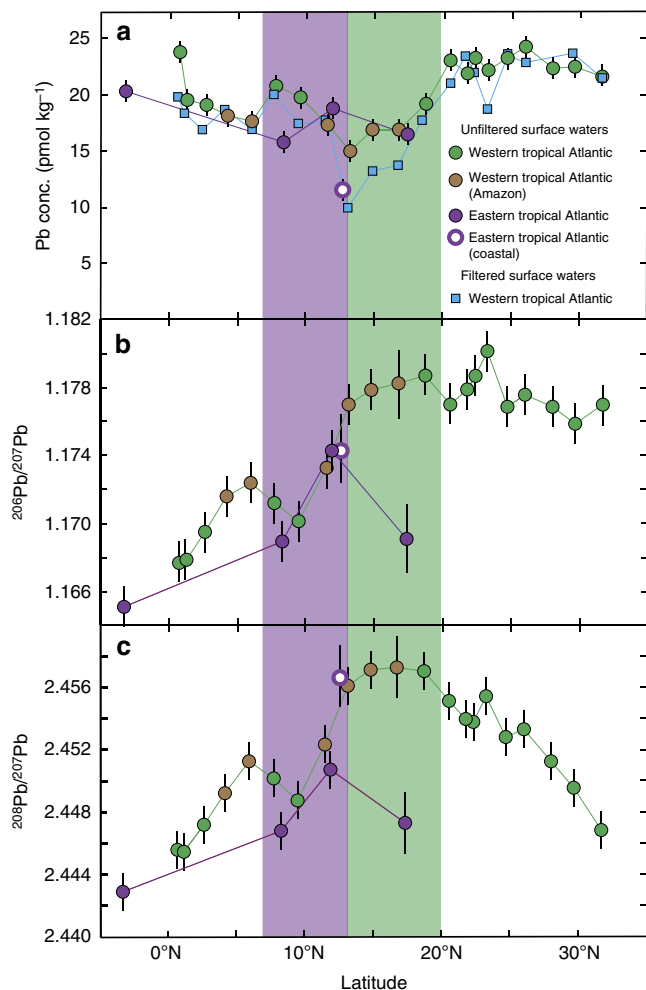


**Figure 2 | Lead concentrations and isotopic compositions results for surface seawater samples.** Panel (a) displays Pb concentration results, while panels (b) and (c) display  $^{206}\text{Pb}/^{207}\text{Pb}$  and  $^{208}\text{Pb}/^{207}\text{Pb}$  ratios respectively, as a function of latitude. Circles denote the results for unfiltered seawater samples, and squares are results for filtered seawater (western Tropical Atlantic only). Green and purple shaded fields denote the position of the North African dust plume during the 64PE321 and D361 cruise, in the western and eastern Tropical Atlantic (WTA and ETA) respectively. Uncertainty assessed through replicate analyses of in-house seawater standards quoted at 1 s.d. for Pb concentrations and 2 s.d. for Pb isotope ratios<sup>66</sup>.

Two important questions follow from these observations. First, whether the higher natural Pb contributions to WTA surface waters are due to mineral dust and/or Amazon River inputs. Second, whether the natural Pb detected in unfiltered seawater samples is primarily in dissolved or particulate form. In the WTA, water masses influenced by mixing with Amazon River water were encountered between 4–6°N and 13–17°N, as identified by decreases in salinity<sup>31,32</sup>. These samples broadly coincide with concurrent maxima in  $^{206}\text{Pb}/^{207}\text{Pb}$  and  $^{208}\text{Pb}/^{207}\text{Pb}$  (Fig. 2b,c), while salinity is negatively correlated with these isotope ratios (Fig. 4a,  $^{206}\text{Pb}/^{207}\text{Pb}$  not shown). It is therefore possible that Amazon River inputs are an important source of natural Pb with high  $^{206}\text{Pb}/^{207}\text{Pb}$  and  $^{208}\text{Pb}/^{207}\text{Pb}$  for these selected samples.

However, these Amazon-influenced surface waters are also characterized by lower total Pb concentrations (15.0–18.1 pmol kg<sup>-1</sup>) than the rest of the samples (19.2–24.3 pmol kg<sup>-1</sup>), with three of the former (13.2–16.8°N)

featuring significant particulate Pb contributions of 18–34% (Fig. 2a, Table 1, Supplementary Table 1). The total Pb concentrations of Amazon-influenced samples display a positive correlation with salinity ( $r^2=0.60$ ,  $P=0.05$ ), indicating that unmixed Amazon outflow water features low Pb contents ( $\ll 10$  pmol kg<sup>-1</sup>; Fig. 4b). This is much lower than dissolved Pb concentrations reported for the Amazon River system ( $\sim 300$ – $800$  pmol kg<sup>-1</sup>)<sup>29</sup>, suggesting that Pb is efficiently removed by biogeochemical processes during mixing with seawater, consistent with previous findings for this and other river systems<sup>9,33</sup>. The Amazon is therefore unlikely to be a significant source of dissolved Pb to the tropical North Atlantic, but may provide minor contributions to the six Amazon influenced samples.

Importantly, the sample at 18.7°N in the WTA features maximum  $^{206}\text{Pb}/^{207}\text{Pb}$  and  $^{208}\text{Pb}/^{207}\text{Pb}$  ratios, but is not affected by mixing with Amazon outflow water (Fig. 2b,c, Fig. 4a). In addition, the latitude of the North African dust plume at the time of sampling along the GA02 section is consistent with the position of concurrent maxima in  $^{206}\text{Pb}/^{207}\text{Pb}$  and  $^{208}\text{Pb}/^{207}\text{Pb}$  ratios observed between 13.2 and 18.7°N in the WTA (Fig. 1b, Fig. 2b,c). Atmospheric deposition of mineral dust is therefore attributed to be the dominant natural source of Pb to these surface waters. The similar Pb concentrations of unfiltered and filtered ( $<0.2\ \mu\text{m}$ ) samples at 18.7°N in the WTA, furthermore suggests that the natural Pb is predominantly in dissolved rather than particulate form (Fig. 2a, Supplementary Table 1).

In the ETA, the maximum contribution of naturally sourced Pb with high  $^{206}\text{Pb}/^{207}\text{Pb}$  and  $^{208}\text{Pb}/^{207}\text{Pb}$  occurs at 11.9°N (Fig. 2b,c). This is further south than in the WTA and consistent with the lower latitude of the North African dust plume in the ETA at the time of sampling. Hence, it can be inferred that atmospheric deposition of mineral dust is the main source of this natural Pb. Comparison of total and particulate ( $>0.45\ \mu\text{m}$ ) Pb concentrations in the ETA indicate particulate Pb contributions of about 7–12% (Supplementary Table 1), confirming that the majority of Pb in these waters is in dissolved form.

Now that we have established that North African mineral dust is the dominant source of natural Pb, isotope mass balance calculations are used to quantitatively estimate the maximum contributions of mineral dust derived  $\text{Pb}_{\text{min}}$  relative to anthropogenic sourced  $\text{Pb}_{\text{anth}}$  in surface waters. The maxima in  $\text{Pb}_{\text{min}}$  contributions are taken to occur in the samples at 11.9°N in the ETA and 18.7°N in the WTA, to avoid any potential influence of Amazon River outflow. The samples from these locations broadly lie on a mixing line between the compositions of North African mineral dust and anthropogenic emissions transported by easterly winds in  $^{206}\text{Pb}/^{207}\text{Pb}$  versus  $^{208}\text{Pb}/^{207}\text{Pb}$  space (Fig. 3). We therefore assume that the Pb in these samples represents a binary mixture of these two sources.

On the basis of a compilation of literature data, the mean isotope compositions of North African mineral dust ( $^{206}\text{Pb}/^{207}\text{Pb}=1.2051$ ,  $^{208}\text{Pb}/^{207}\text{Pb}=2.4972$ ) and anthropogenic Pb transported by easterly winds ( $^{206}\text{Pb}/^{207}\text{Pb}=1.1532$ ,  $^{208}\text{Pb}/^{207}\text{Pb}=2.4304$ ) are used to define a mixing line between these two endmembers (Fig. 3; Supplementary Note 2). Comparison of our data with this mixing line indicates that the seawater samples feature maximum  $\text{Pb}_{\text{min}}$  contributions of approximately 30 to 50%. The use of mean Pb isotope ratios to define the endmembers is thereby justified by the longer residence time of Pb in ocean surface waters (approximately months to years<sup>13,14</sup> see the ‘Discussion’ section) compared with the atmosphere (approximately days<sup>34</sup>), because this will integrate the variable isotope composition of atmospheric inputs towards average values.

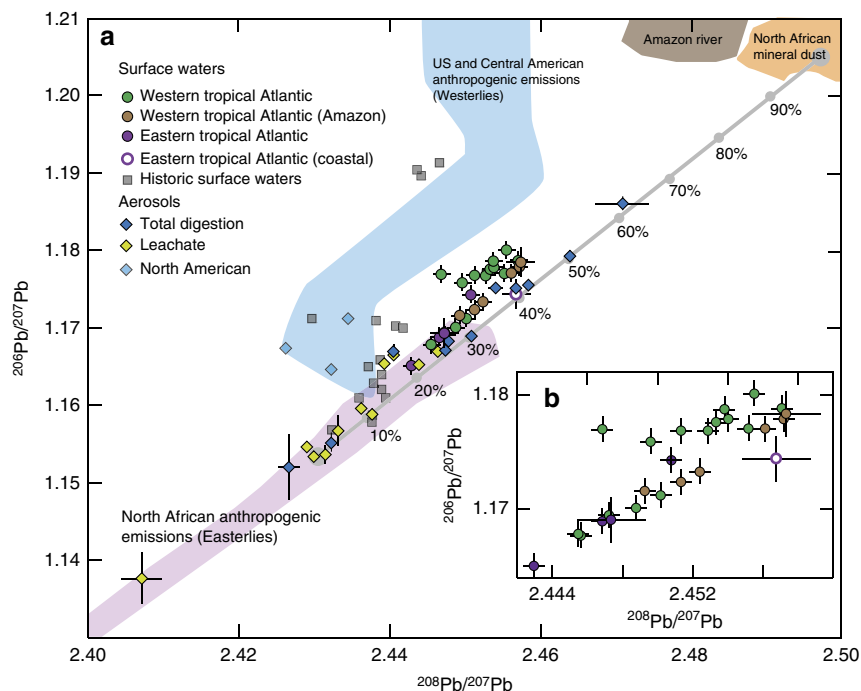


**Figure 3 | A plot of  $^{206}\text{Pb}/^{207}\text{Pb}$  versus  $^{208}\text{Pb}/^{207}\text{Pb}$  for surface water and aerosol samples for source assessment.** Panel (a)  $^{206}\text{Pb}/^{207}\text{Pb}$  versus  $^{208}\text{Pb}/^{207}\text{Pb}$  for unfiltered surface seawater from GEOTRACES sections GA02 (2nd leg) and GA06 and aerosols (total digests and leachates; GA06). Shown for comparison are the Pb isotope compositions of (1) the major potential Pb sources to the tropical Atlantic (coloured fields<sup>23–30</sup>) with recent North American aerosols denoted by light blue diamonds<sup>11</sup>, (2) surface seawaters collected in the region during the 1980s and 1990s (grey squares<sup>8,9</sup>), as well as (3) a mixing line between anthropogenic Pb ( $\text{Pb}_{\text{anth}}$ ) transported by easterly winds and mineral dust derived Pb ( $\text{Pb}_{\text{min}}$ ). Inset panel (b), displays an enlargement of  $^{206}\text{Pb}/^{207}\text{Pb}$  versus  $^{208}\text{Pb}/^{207}\text{Pb}$  ratios for unfiltered surface seawater only. Quoted uncertainties (2 s.d.) for the seawater and aerosol data are assessed as through replicate analyses of in-house seawater standards<sup>66</sup> (seawater) or by propagation of uncertainty associated with blank corrections and measurement protocols (aerosols).

**Sources of Pb to the atmosphere.** On the basis of results of air mass back trajectory analyses<sup>35</sup>, the aerosol samples were split into three groups, originating from North Africa ('North African'), Algeria ('Algerian') and samples collected within/south of the ITCZ. The latter group did not encounter land in the 5 days preceding collection ('Oceanic') (Supplementary Figs 1–3). The 'Algerian' samples were distinguished from the remaining 'North African' aerosols, as leaded petrol was still available in Algeria at the time of sampling in 2011 (ref. 16). Every aerosol sample was subjected to both total digestion and a leaching procedure to determine the component of each sample that is potentially soluble in the marine environment (see the 'Methods' section). The Pb and Al concentrations as well as the Pb isotope compositions for the total digests and leachates are presented in Table 2.

Two independent approaches were applied to estimate the relative proportions of  $\text{Pb}_{\text{min}}$  and  $\text{Pb}_{\text{anth}}$  in the total aerosol digests: an isotope mass balance calculation and an approach based on crustal enrichment factors ( $\text{EF}_{\text{crust}}$ ). The first calculation used the Pb isotope compositions of the aerosol samples, which are in accord with a mixing relationship in  $^{206}\text{Pb}/^{207}\text{Pb}$  versus  $^{208}\text{Pb}/^{207}\text{Pb}$  space between  $\text{Pb}_{\text{anth}}$  transported by easterly winds, and  $\text{Pb}_{\text{min}}$  from North African mineral dust (Fig. 3). In detail, the Pb isotope compositions of the total digests trend towards mineral dust compositions while the leachate samples overlap the range of  $\text{Pb}_{\text{anth}}$  transported by easterly winds ( $^{206}\text{Pb}/^{207}\text{Pb} = 1.1338\text{--}1.1666$  and  $^{208}\text{Pb}/^{207}\text{Pb} = 2.4037\text{--}2.4466$ ). This is consistent with the findings of previous studies, showing that  $\text{Pb}_{\text{anth}}$  is much more soluble than  $\text{Pb}_{\text{min}}$  (refs 36–42). The isotope composition of each leachate is therefore taken as representative for  $\text{Pb}_{\text{anth}}$  in the corresponding total digest. The relatively large isotopic variability of the leachates is indicative of significant compositional heterogeneity for  $\text{Pb}_{\text{anth}}$  in

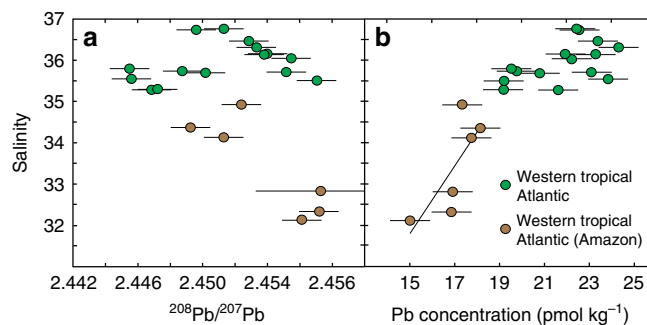


**Figure 4 | Comparison of the Pb contents and isotope composition of Amazon influenced to the remainder of WTA surface waters.** Salinity versus  $^{208}\text{Pb}/^{207}\text{Pb}$  ratios (panel a), and Pb concentrations (panel b) for unfiltered surface seawater samples collected in the western tropical Atlantic (GEOTRACES section GA02, 2nd leg). The samples affected by mixing with Amazon River water are distinguished as brown circles, while other samples are marked in green. Quoted uncertainties in  $^{208}\text{Pb}/^{207}\text{Pb}$  ratios (2 s.d.) and Pb concentrations (1 s.d.) are assessed through replicate analyses of in-house seawater standards<sup>66</sup>.

the atmosphere over short timescales (approximately days). Presumably this reflects the short residence time of several days for these atmospheric aerosols<sup>34</sup>.

On the basis of these systematics, the isotope mass balance approach assumes the total digests contain a binary mixture of  $\text{Pb}_{\text{min}}$  and  $\text{Pb}_{\text{anth}}$  transported by easterly winds, whereby the isotope composition of  $\text{Pb}_{\text{anth}}$  is represented by the corresponding leachates. Using the mean  $^{206}\text{Pb}/^{207}\text{Pb}$  ratio of North

**Table 2 | Elemental concentrations and Pb isotope compositions for aerosols collected in the eastern tropical Atlantic along GEOTRACES section GA06.**

Sample ID	Latitude* (°N)	Longitude* (°W)	AMBT Group†	[Pb] (ng m <sup>-3</sup> )‡	Fractional solubility§ (%)	[Al] (ng m <sup>-3</sup> )	EF <sub>crust</sub>	<sup>206</sup> Pb/ <sup>204</sup> Pb <sup>¶</sup> ± 2 s.d.	<sup>206</sup> Pb/ <sup>207</sup> Pb <sup>¶</sup> ± 2 s.d.	<sup>208</sup> Pb/ <sup>207</sup> Pb <sup>¶</sup> ± 2 s.d.	Pb <sub>min</sub> proportion estimates (%) <sup>#</sup>	[Pb] <sub>anth</sub> (ng m <sup>-3</sup> ) <sup>**</sup>
ISO-5 <sub>Total</sub>	13.13	17.97	NA	1.960 ± 0.008	18.5 ± 0.4	5,048	1.86 ± 0.01	18.5819 ± 0.0176	1.1860 ± 0.0010	2.4710 ± 0.0036	61.5/53.7	0.76/0.91
ISO-5 <sub>Leach</sub>	12.55	18.84		0.362 ± 0.008		39		18.2426 ± 0.0095	1.1668 ± 0.0003	2.4462 ± 0.0005		
ISO-7 <sub>Total</sub>	12.55	18.87	Al	4.113 ± 0.011	47.2 ± 0.3	1,935	10.19 ± 0.03	18.2792 ± 0.0087	1.1691 ± 0.0001	2.4508 ± 0.0004	22.3/9.8	3.2/3.7
ISO-7 <sub>Leach</sub>	12.57	21.82		1.941 ± 0.011		32		18.1024 ± 0.0087	1.1587 ± 0.0002	2.4378 ± 0.0003		
ISO-8 <sub>Total</sub>	12.57	21.82	NA	1.308 ± 0.009	17.2 ± 0.7	3,482	1.80 ± 0.01	18.4649 ± 0.0088	1.1792 ± 0.0002	2.4638 ± 0.0007	50.3/55.5	0.65/0.58
ISO-8 <sub>Leach</sub>	12.57	23.76		0.225 ± 0.009		15		18.0165 ± 0.0214	1.1536 ± 0.0012	2.4314 ± 0.0004		
ISO-11 <sub>Total</sub>	12.54	23.92	Al	0.506 ± 0.016	42.4 ± 3.4	1,128	2.15 ± 0.07	18.3925 ± 0.0086	1.1750 ± 0.0001	2.4567 ± 0.0004	21.5/46.5	0.40/0.27
ISO-11 <sub>Leach</sub>	9.46	25.66		0.214 ± 0.016		9		18.0679 ± 0.0341	1.1567 ± 0.0020	2.4331 ± 0.0005		
ISO-12 <sub>Total</sub>	8.67	25.62	Al	2.941 ± 0.012	41.5 ± 0.4	3,891	3.62 ± 0.01	18.2671 ± 0.0089	1.1682 ± 0.0002	2.4478 ± 0.0004	19.0/27.6	2.4/2.1
ISO-12 <sub>Leach</sub>	1.02	25.33		1.220 ± 0.012		30		18.0990 ± 0.0093	1.1597 ± 0.0002	2.4360 ± 0.0003		
ISO-14 <sub>Total</sub>	-0.80	25.31	Oc	0.193 ± 0.005	61.3 ± 3.2	137	6.74 ± 0.18	18.2323 ± 0.0235	1.1669 ± 0.0010	2.4405 ± 0.0007	2.1/14.8	0.19/0.16
ISO-14 <sub>Leach</sub>	-7.00	25.00		0.118 ± 0.005		5		18.2600 ± 0.0114	1.1666 ± 0.0006	2.4405 ± 0.0004		
ISO-16 <sub>Total</sub>	-7.15	24.99	Oc	0.117 ± 0.006	82.7 ± 6.4	68	8.21 ± 0.41	18.0064 ± 0.0766	1.1520 ± 0.0043	2.4265 ± 0.0015	25.3/12.2	0.09/0.10
ISO-16 <sub>Leach</sub>	-3.15	25.54		0.097 ± 0.006		2		17.7103 ± 0.0589	1.1376 ± 0.0033	2.4070 ± 0.0027		
ISO-19 <sub>Total</sub>	-2.96	25.61	Oc	0.552 ± 0.007	54.5 ± 1.5	728	3.63 ± 0.05	18.3829 ± 0.0101	1.1751 ± 0.0003	2.4540 ± 0.0008	24.6/27.5	0.42/0.40
ISO-19 <sub>Leach</sub>	1.68	26.25		0.301 ± 0.007		15		18.2098 ± 0.0101	1.1654 ± 0.0004	2.4391 ± 0.0003		
ISO-21 <sub>Total</sub>	1.81	26.29	NA	0.932 ± 0.006	41.1 ± 0.6	1,527	2.93 ± 0.02	18.4072 ± 0.0088	1.1756 ± 0.0002	2.4583 ± 0.0005	26.0/34.2	0.69/0.61
ISO-21 <sub>Leach</sub>	6.74	27.80		0.383 ± 0.006		28		18.2042 ± 0.0092	1.1652 ± 0.0002	2.4438 ± 0.0004		
ISO-23 <sub>Total</sub>	6.84	27.84	NA	0.500 ± 0.006	63.0 ± 1.3	667	3.59 ± 0.04	18.2453 ± 0.0119	1.1669 ± 0.0004	2.4473 ± 0.0005	24.8/27.9	0.38/0.36
ISO-23 <sub>Leach</sub>	11.31	28.86		0.314 ± 0.006		13		18.0142 ± 0.0122	1.1547 ± 0.0005	2.4292 ± 0.0004		
ISO-25 <sub>Total</sub>	11.45	28.89	NA	0.230 ± 0.004	73.7 ± 2.2	74	14.90 ± 0.27	18.0242 ± 0.0262	1.1552 ± 0.0013	2.4322 ± 0.0004	4.8/6.7	0.22/0.21
ISO-25 <sub>Leach</sub>	17.42	28.38		0.170 ± 0.004		2		18.0048 ± 0.0153	1.1534 ± 0.0008	2.4298 ± 0.0004		

\*Latitudes/longitudes between which samples were collected.

†AMBT = air mass back trajectory group, NA = North African, Al = Algerian, Oc = oceanic (Supplementary Figs 1-3).

‡Atmospheric Pb concentration, uncertainty estimated by propagation of the sampling blank uncertainty (1 s.d., see Methods).

§Fractional solubility of Pb in leaching procedure (equation (4)); uncertainty estimated by propagating the uncertainties (1 s.d.) of the atmospheric Pb concentrations from analyses of the leachates and total aerosol digests (see Methods).

||Crustal enrichment factors (equation (1)); uncertainty based on the uncertainty (1 s.d.) of atmospheric concentrations (see text).

¶Pb isotope ratios are corrected for the Pb content and isotope composition of the sampling blank, with uncertainties (2 s.d.) assessed as described in the Methods section.

#Estimated proportions of Pb<sub>min</sub> in the total digests calculated using the isotope mass balance/EF approaches.

\*\*Atmospheric concentrations of Pb<sub>anth</sub> estimated based on Pb<sub>min</sub> proportions calculated using the isotope mass balance/EF approaches (equation (3)).

African mineral dust from the literature as Pb<sub>min</sub> endmember (<sup>206</sup>Pb/<sup>207</sup>Pb = 1.2051, Supplementary Table 5), and the <sup>206</sup>Pb/<sup>207</sup>Pb ratio of each leachate to represent Pb<sub>anth</sub>, the proportion of Pb<sub>min</sub> in each total digest is calculated from the isotope mass balance (Supplementary Note 2). Importantly, use of <sup>208</sup>Pb/<sup>207</sup>Pb ratios for these calculations yields almost identical results (Supplementary Fig. 4). In detail, estimated Pb<sub>min</sub> proportions range between 2 and 61%, with uncertainty arising mainly from the potentially variable isotope composition of the Pb<sub>min</sub> endmember (Table 2). The latter is assessed by propagating the full range of compiled <sup>206</sup>Pb/<sup>207</sup>Pb data for North African mineral dust (1.2000–1.2167) through the calculations. This yields Pb<sub>min</sub>% uncertainties of up to about ± 10%, which increase with increasing Pb<sub>min</sub> proportions (Supplementary Fig. 5).

The second approach using EF<sub>crust</sub> values provides additional, independent constraints on the relative proportions of Pb<sub>min</sub> and Pb<sub>anth</sub> in the total digests. Crustal enrichment factors are a common method of assessing the relative importance of mineral dust and anthropogenic emissions to atmospheric Pb budgets (for example, see refs <sup>20,36,43–45</sup>). They are typically calculated by normalizing the Pb/Al ratio of an aerosol sample (Pb/Al<sub>sample</sub>) to a reference ratio for the upper continental crust, Pb/Al<sub>ucc</sub> (equation (1)).

$$EF_{crust} = \left( \frac{Pb/Al_{sample}}{Pb/Al_{ucc}} \right) \quad (1)$$

The main uncertainty of this approach is how well the chosen crustal reference ratio characterizes the mineral dust. Such uncertainty has led to the convention of applying EF<sub>crust</sub> values in a qualitative manner, whereby only EF<sub>crust</sub> values > 5 or 10 are interpreted to represent definite enrichments of Pb<sub>anth</sub> (for example, see refs <sup>36,43–45</sup>). Using Pb/Al<sub>ucc</sub> = 2.09 × 10<sup>-4</sup> from Rudnick & Gao<sup>46</sup>, the EF<sub>crust</sub> values for the total digests range between 1.9 and 14.9 (Table 2). Hence, the majority of the aerosol samples would not be considered significantly enriched in

Pb<sub>anth</sub> following this conventional approach. However, the isotope data clearly shows that they contain substantial proportions of Pb<sub>anth</sub> (Fig. 3).

To fully compare the constraints on aerosol Pb<sub>min</sub> proportions provided by the isotope data and EF<sub>crust</sub> values, and to assess the suitability of the chosen Pb/Al<sub>ucc</sub> reference ratio, Pb<sub>min</sub> proportions in the total digests are quantitatively estimated following equation (2), where Al<sub>total</sub> and Pb<sub>total</sub> denote the atmospheric Al and Pb concentrations derived from the total digests. This approach yields Pb<sub>min</sub> proportions for the total digests of 7 to 54%, in good agreement with the results of the isotope mass balance approach (Table 2, Fig. 5a). Importantly, this agreement suggests that the Pb<sub>min</sub> proportion estimates are reasonably robust, and that the chosen crustal reference value suitably characterizes the Pb/Al ratio of North African mineral dust. There are a few exceptions to this, notably sample ISO-11 for which the results of the two approaches differ by about 25%. This discrepancy is likely due to an unusual natural Pb/Al ratio of the mineral dust as a result of mineralogical variability. The isotope mass balance calculations are hence more likely to provide robust estimates of Pb<sub>min</sub> proportions.

$$Pb_{min}(\%) = \left[ \frac{(Al_{total} \times Pb/Al_{ucc})}{Pb_{total}} \right] \times 100 \quad (2)$$

In summary, both approaches demonstrate that the proportions of Pb<sub>min</sub> and Pb<sub>anth</sub> in the atmosphere are highly variable over timescales of several days. Most likely, this variability reflects differences in the emission and transport of these two distinct Pb sources. Atmospheric Al concentrations are commonly used as a proxy for the concentration of mineral dust in the atmosphere, with the assumption that the latter has a Al content of 8% (w/w) (for example, see refs <sup>20,43,44</sup>). Atmospheric Al abundances range over three orders of magnitude from 68 to 5,048 ng m<sup>-3</sup>, corresponding to atmospheric mineral dust concentrations of about 0.9–63 μg m<sup>-3</sup>. Estimated Pb<sub>min</sub> proportions generally increase with increasing Al concentrations (Fig. 5b), which

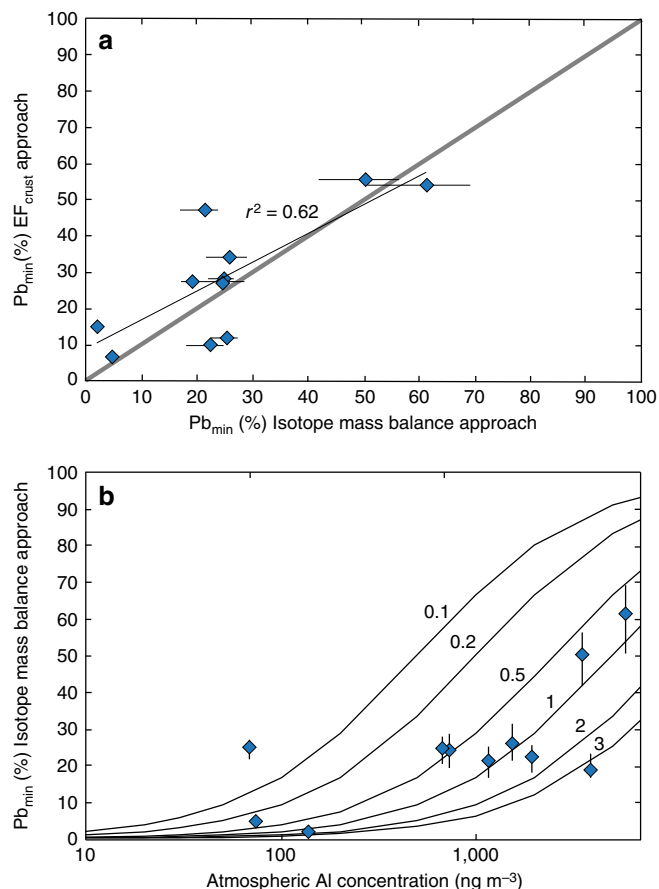


**Figure 5 | Results of mineral dust derived Pb proportion estimates for the aerosol total digests.** (a) comparison between the proportions of mineral dust derived Pb ( $Pb_{min}$ ) in the total digests of aerosol samples, as estimated using the isotope mass balance versus the enrichment factor (EF) based approaches. The grey line denotes a 1:1 relationship. Panel (b) the proportion of  $Pb_{min}$  in the total aerosol digests estimated using the isotope mass balance approach plotted versus atmospheric Al concentrations, as a proxy for atmospheric mineral dust abundance. The black contours denote constant anthropogenic Pb ( $Pb_{anth}$ ) concentrations for the atmosphere (in  $ng\ m^{-3}$ ), calculated for mineral dust with Pb/Al ratio of  $2.09 \times 10^{-4}$  (ref. 44). Uncertainty in the  $Pb_{min}$  proportion estimates by the isotope mass balance based approach is assessed by propagation of the full range of  $^{206}Pb/^{207}Pb$  ratios compiled for North African mineral dust through the calculations.

suggests that the observed variability in  $Pb_{min}$  proportions is largely driven by highly variable atmospheric mineral dust concentrations. This conclusion is consistent with the findings of previous studies in regions strongly affected by both mineral dust and anthropogenic emissions<sup>36,43,44</sup>. However, there is considerable scatter in the trend of Fig. 5b, presumably reflecting variations in atmospheric  $Pb_{anth}$  concentrations.

Atmospheric  $Pb_{anth}$  concentrations are calculated using the estimated  $Pb_{min}$  proportions and total atmospheric Pb concentrations ( $Pb_{total}$ ) (equation (3)). Note that using the  $Pb_{min}$  proportions determined by either the isotope mass balance or the  $EF_{crust}$  approach yields similar results (Supplementary Fig. 6). Two of the samples from the ‘Algerian’ group exhibit anomalously high atmospheric  $Pb_{anth}$  concentrations of 2.4 and  $3.2\ ng\ m^{-3}$ , presumably reflecting the continued use of leaded petrol in Algeria at the time of sampling<sup>16</sup> (Table 2). Atmospheric  $Pb_{anth}$  concentrations for the remainder of the samples range

between  $0.1\text{--}0.8\ ng\ m^{-3}$ .

$$Pb_{anth}(ng\ m^{-3}) = Pb_{total} - [(Pb_{min}(\%)/100) \times Pb_{total}] \quad (3)$$

### Solubility of anthropogenic and mineral dust derived Pb.

Previous studies concluded that  $Pb_{anth}$  is more soluble than  $Pb_{min}$  in natural waters (precipitation and seawater) and attributed this to differences in solid state speciation<sup>36–42</sup>. This solubility difference is also demonstrated here by the anthropogenic isotope compositions of the leachates (Fig. 3). The fraction of Pb released by leaching, calculated relative to the Pb concentrations released from total digestion and expressed as a percentage (equation (4)), ranges between 19 and 83% (Table 2). The estimated  $Pb_{min}$  proportions in the total digests are thereby negatively correlated with the fractional solubility, with a gradient of  $-0.9$  ( $r^2 = 0.56$ ,  $P = 0.009$ ) (Fig. 6). This gradient suggests that  $Pb_{anth}$  is approximately 100 times more soluble than  $Pb_{min}$  during leaching, that is,  $\sim 1\%$  decrease in fractional solubility per  $1\%$  increase in  $Pb_{min}$  proportions in the aerosol. Extrapolation of this trend yields fractional solubilities of  $\sim 70\%$  and  $\sim 15\%$  for the pure  $Pb_{anth}$  and  $Pb_{min}$  endmembers, respectively. The apparent negative solubility for the  $Pb_{min}$  endmember is obviously unrealistic. The latter result is, however, still significant because it likely reflects scavenging of both  $Pb_{anth}$  and  $Pb_{min}$  following initial aerosol dissolution during leaching, a type of behaviour that has been documented previously<sup>36–39,47</sup>.

$$\text{Fractional solubility}(\%) = (Pb_{Leach}/Pb_{Total}) \times 100 \quad (4)$$

### Discussion

This is the first time a significant proportion of up to 30–50% of Pb from a natural source has been detected in Atlantic surface waters. With the exception of the potentially natural Pb contributions observed in surface waters of the remote Southern Ocean<sup>48</sup>, this finding also applies to the entire global ocean. We suggest that our observation reflects the nearly complete phase-out of leaded petrol, and is a testament to the success of efforts to reduce anthropogenic Pb emissions in regions surrounding the Atlantic, which started over 40 years ago<sup>49</sup>.

An important observation is that the locations determined for the maximum  $Pb_{min}$  proportions in surface waters are consistent with the position of the North African dust plume during the two cruises (Fig. 1b,c, Fig. 2). This may indicate that seasonal changes in surface water Pb inventories of this region occur in response to the changing position of the dust plume. Alternatively, these features may be perennial, reflecting the locations of highest annual mineral dust fluxes. For the ETA this is potentially the case, as mineral dust deposition rates are highest in this region during the boreal winter, when the dust plume is situated at lower latitudes<sup>20,22</sup>. However, the magnitude of mineral dust transport to sites in the WTA by the dust plume is relatively consistent throughout the seasonal cycle<sup>18</sup>. Ocean circulation can act to redistribute and mix the different atmospheric Pb inputs to surface waters. A significant role for large-scale redistribution of surface ocean Pb in the tropical North Atlantic is negated, however, by the well-defined atmospheric input signals, which coincide with the changing positions of the dust plume.

If this interpretation is correct, it implies that the residence time of Pb in ocean surface waters in this region may be on the order of months, to produce and preserve such spatially distinct and seasonal isotope signatures. In particular, the residence time must be long enough to allow highly variable atmospheric inputs to be averaged to produce the observed smooth and systematic spatial variability in Pb isotope compositions (Fig. 2). However, it must also be short enough to avoid any ‘memory’ of previous dust

plume positions and redistribution of this input signal by ocean circulation.

Our results may therefore suggest a substantially shorter residence time for Pb in ocean surface waters of the studied area than the value of several years that is typically assumed, based on investigations of oligotrophic regions of the ocean<sup>13,14</sup>. Although this interpretation requires validation by further studies, we can speculate that enhanced scavenging rates of Pb in the tropical Atlantic surface waters could be related to the large inputs of mineral dust in this region. Mineral dust is expected to be a sink as well as a source of Pb through re-adsorption of Pb onto the surfaces of mineral dust particles<sup>36–39,47</sup> (Fig. 6) and by acting as ballast, increasing the rate at which particulate organic material is removed from the ocean surface<sup>50</sup>.

The detection of  $Pb_{min}$  in the ocean surface also enables the study of factors that govern its atmospheric flux. Such insights will prove useful in assessing how changes in anthropogenic and natural Pb fluxes may affect the Pb budgets of other oceanic regions. The relative proportion of  $Pb_{min}$  and  $Pb_{anth}$  in ocean surface waters (os) will depend on their relative atmospheric concentrations (at), deposition velocities (dp) and solubilities (sol; equation (5)).

$$\left(\frac{Pb_{min}}{Pb_{anth}}\right)_{os} = \left(\frac{Pb_{min}}{Pb_{anth}}\right)_{at} \times \left(\frac{Pb_{min}}{Pb_{anth}}\right)_{dp} \times \left(\frac{Pb_{min}}{Pb_{anth}}\right)_{sol} \quad (5)$$

The results of our leaching procedure suggest that  $\left(\frac{Pb_{min}}{Pb_{anth}}\right)_{sol} \approx 0.01$  (Fig. 6). However, given the uncertainty about how well the leaching conditions replicate relevant natural processes, we derive a more conservative constraint of  $\left(\frac{Pb_{min}}{Pb_{anth}}\right)_{sol} \leq 0.1$ . In any case, this solubility difference requires the atmospheric deposition of  $Pb_{min}$  to greatly exceed that of  $Pb_{anth}$  to reproduce the large observed  $Pb_{min}$  proportions (30–50%) in ocean surface waters. In the following, we investigate whether realistic relative atmospheric concentrations of  $Pb_{min}$  and  $Pb_{anth}$  alone can be responsible for the higher  $Pb_{min}$  deposition rates that are needed, or whether the preferential deposition of  $Pb_{min}$  over  $Pb_{anth}$  is also required (that is, different deposition velocities).

Over short timescales (approximately days), the relative proportions of  $Pb_{min}$  and  $Pb_{anth}$  in the atmosphere are highly variable ( $\sim 2$ –60%  $Pb_{min}$ ), which can be predominantly ascribed to variations in atmospheric mineral dust concentrations (Fig. 5). To investigate the impact of such changes on surface water Pb budgets, it is necessary to constrain the relative atmospheric concentrations of  $Pb_{min}$  and  $Pb_{anth}$ , averaged over the residence time of Pb in ocean surface waters. The Pb residence time in surface waters of this region may be as short as several months (see above), whereby the maximum  $Pb_{min}$  contributions to surface waters possibly relate to the seasonal migration of the North African dust plume. During the seasonal dusty periods, typical monthly averaged atmospheric mineral dust concentrations at sites in the ETA and WTA are about 20–50  $\mu\text{g m}^{-3}$  (refs 18,20). These values likely represent the highest relevant atmospheric mineral dust concentrations, since averaging over longer timescales will include less dusty periods. Assuming an Al concentration of 8% and  $Pb/Al = 2.09 \times 10^{-4}$  for mineral dust, this corresponds to atmospheric  $Pb_{min}$  concentrations of 0.4–0.8  $\text{ng m}^{-3}$ . Coupled with the median atmospheric  $Pb_{anth}$  concentration (0.4  $\text{ng m}^{-3}$ ) determined from the aerosol total digests (omitting the two anomalously values for ‘Algerian’ samples), this results in  $\left(\frac{Pb_{min}}{Pb_{anth}}\right)_{at}$  ratios of 1–2 (Table 3). Hence, even during the dustiest periods of the year, the average atmospheric  $Pb_{min}$  concentrations are unlikely to greatly exceed those of  $Pb_{anth}$ . A more conservative approach can be adopted by coupling the lowest estimated atmospheric  $Pb_{anth}$  concentrations

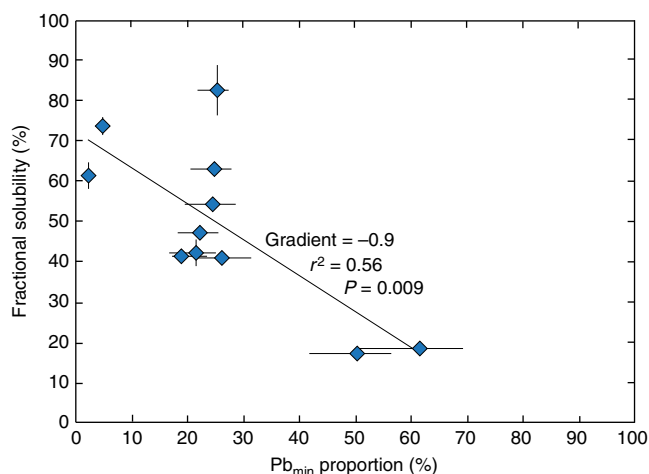


**Figure 6 | The relationship between solubility and proportion of mineral dust derived Pb.**

Results of the fractional solubility of Pb in the leaching procedure relative to the total digests as a function of estimated proportion of mineral dust derived Pb in each aerosol sample. Displayed  $Pb_{min}$  proportion estimates are derived using the isotope mass balance approach, with uncertainty assessed by propagation of the full range of  $^{206}\text{Pb}/^{207}\text{Pb}$  ratios compiled for North African mineral dust through the calculations. Uncertainty of the fractional solubility estimates (1 s.d.) is assessed by propagation of the variability of the sampling blank through the calculation.

of 0.1  $\text{ng m}^{-3}$  with the highest reasonable average atmospheric  $Pb_{min}$  abundance of 0.8  $\text{ng m}^{-3}$ , which sets a maximum possible  $\left(\frac{Pb_{min}}{Pb_{anth}}\right)_{at}$  ratio of 8.

Particles suspended in the atmosphere are transferred to ocean surface waters through either wet or dry deposition. The main removal mechanism in dry deposition is gravitational settling, which becomes less efficient with decreasing particle size<sup>34</sup>. Anthropogenic enrichments of trace metals in aerosols are known to be concentrated in smaller particles ( $\sim 0.1$ –1  $\mu\text{m}$ ) than mineral dust ( $\sim 2$   $\mu\text{m}$  following transport to the WTA)<sup>51,52</sup>. Models therefore parameterize mineral dust to be preferentially deposited over finer anthropogenic particles during dry deposition and this is supported by field observations<sup>22,36,53–55</sup>. In contrast, wet deposition is considered to efficiently remove both mineral dust and finer anthropogenic particles<sup>53</sup>. Therefore, the relative deposition velocities of  $Pb_{min}$  and  $Pb_{anth}$  depend on the relative importance of wet versus dry deposition, which in turn is determined by the amount of precipitation in the relevant region. In our study area, the ITCZ marks a location of intense precipitation (up to 10  $\text{mm day}^{-1}$ , annual average), while the area immediately to the north is characterized by much lower precipitation rates (0–1  $\text{mm day}^{-1}$ , annual average)<sup>56</sup>. Consequently, wet deposition is the dominant deposition mode in the ITCZ<sup>57</sup>, whereas further north, where the relative maxima in  $Pb_{min}$  contributions to seawater are observed, dry deposition is estimated to account for 95% of the atmospheric dust flux to the ocean<sup>45</sup>.

Aluminium concentration data for surface seawater suggests that mineral dust derived trace metals fluxes are larger to the north ( $>30^\circ\text{N}$ ) and south ( $<10^\circ\text{N}$ ) of the observed relative maxima in  $Pb_{min}$  contributions to surface waters<sup>32,58,59</sup>. Most likely, this reflects more efficient dust removal in regions where wet deposition is important or dominant. Hence, the observed geographic positions of aerosol fluxes with the highest  $Pb_{min}$  proportions is likely not coincident with the highest absolute fluxes of  $Pb_{min}$  to this region. This suggests that preferential deposition of  $Pb_{min}$  over  $Pb_{anth}$  by dry deposition is a key factor



**Table 3 | Results of sensitivity test on  $(Pb_{min}/Pb_{anth})_{dp}$  using constraints for  $(Pb_{min}/Pb_{anth})_{at}$  and  $(Pb_{min}/Pb_{anth})_{sol}$  outlined in the main text.**

$(Pb_{min}/Pb_{anth})_{sol}$	$(Pb_{min}/Pb_{anth})_{at}$		
	Representative		Maximum
	1	2	8
0.01	30.0–50.0	15.0–25.0	3.8–6.3
0.02	15.0–25.0	7.5–12.5	<b>1.9–3.1</b>
0.03	10.0–16.7	5.0–8.3	<b>1.3–2.1</b>
0.04	7.5–12.5	3.8–6.3	<b>0.9–1.6</b>
0.05	6.0–10.0	3.0–5.0	<b>0.8–1.3</b>
0.06	5.0–8.3	2.5–4.2	<b>0.6–1.0</b>
0.07	4.3–7.1	2.1–3.6	<b>0.5–0.9</b>
0.08	3.8–6.3	<b>1.9–3.1</b>	<b>0.5–0.8</b>
0.09	3.3–5.6	<b>1.7–2.8</b>	<b>0.4–0.7</b>
0.10	3.0–5.0	<b>1.5–2.5</b>	<b>0.4–0.6</b>

The values in each cell corresponds to the required  $(Pb_{min}/Pb_{anth})_{dp}$  ratios required to produce  $(Pb_{min}/Pb_{anth})_{os} = 0.3–0.5$ . The part of the domain which does not require preferential deposition of  $Pb_{min}$  over  $Pb_{anth}$  because the calculations yield  $(Pb_{min}/Pb_{anth})_{dp} < 2$ , is highlighted in bold. We argue that  $(Pb_{min}/Pb_{anth})_{at}$  ratios of 1 to 2 are likely for the tropical North Atlantic during the dustiest periods of the year, while a ratio of 8 represents an absolute maximum.

in producing the observed high proportions of  $Pb_{min}$  in the ocean surface. To test this hypothesis, we carried out a sensitivity test, which investigates the  $(Pb_{min}/Pb_{anth})_{dp}$  ratios needed to produce the observed values of  $(Pb_{min}/Pb_{anth})_{os} = 0.3–0.5$  (equation (5)), using the previously derived boundary conditions of  $(Pb_{min}/Pb_{anth})_{at} = 1–2$  and  $< 8$ , and  $(Pb_{min}/Pb_{anth})_{sol} \leq 0.1$  (Table 3). The results of the test support the hypothesis, as they demonstrate that dry deposition, characterized by preferential removal of  $Pb_{min}$  over  $Pb_{anth}$  with  $(Pb_{min}/Pb_{anth})_{dp} > 1$ , is required for most of the investigated parameter space (Table 3).

Climatological models of aerosol deposition to open ocean surface waters have parameterized dry deposition velocities as  $0.02–0.2 \text{ cm s}^{-1}$  and  $0.4–2 \text{ cm s}^{-1}$  for fine ( $< 1 \mu\text{m}$ ; anthropogenic) and coarse particles ( $> 1 \mu\text{m}$ ; mineral dust) respectively, which corresponds to  $(Pb_{min}/Pb_{anth})_{dp}$  of about 10–20 (refs 22,36,54,54). The dominance of aerosol flux by dry deposition, therefore likely increases the proportions of  $Pb_{min}$  in surface water by a factor of 10 to 20, relative to a wet deposition dominated flux. Hence, the observed 30–50% proportion of  $Pb_{min}$  in surface waters would likely only be 2–5% in a wet deposition dominated regime, and would be undetectable using the isotopic data. In this context, it is important to emphasize that the dominance of dry deposition is relatively unusual, with wet deposition estimated to dominate the atmospheric aerosol flux to the global ocean<sup>60</sup>.

In summary, significant amounts of up to 30–50% of Pb from natural sources (mineral dust) were detected in ocean surface waters of the tropical North Atlantic. This finding reflects the now almost complete global phase-out of leaded petrol and can be viewed as a success of environmental policy. Relative maxima in  $Pb_{min}$  contributions to surface waters occur in restricted latitudinal bands, and their location and magnitude are influenced by the position of the North African dust plume, which features the highest atmospheric mineral dust concentrations observed for the global ocean, and the dominance of dry deposition which favors the deposition of  $Pb_{min}$  over  $Pb_{anth}$ . Acting together, these factors are relatively specific to this region of the ocean. The observation that  $Pb_{anth}$  still contributes up to 50% of the Pb in these surface waters hence suggests that Pb emissions from other anthropogenic activities, such as the combustion of unleaded petrol, coal burning and metal smelting, remain the dominant sources of Pb to the ocean, even following the global cessation of leaded petrol usage<sup>1,4</sup>.

## Methods

**Sample collection.** Samples utilized for this study were collected during the second leg of the GEOTRACES GA02 section on the *RV Pelagia* (cruise 64PE321, 11th June–8th July, 2010) and during the GEOTRACES GA06 section on the *RRS Discovery* (cruise D361, 7th February–19th March, 2011). Unfiltered surface waters (2–3 m depth) were collected while underway, during both of these cruises, using a towed ‘fish’. Within trace-metal-clean environments on the ships, samples for total Pb concentration and isotope composition analysis were subsequently transferred into pre-cleaned LDPE bottles and triple bagged. Back on shore, within a clean environment at Imperial College London, samples were subsequently acidified to an approximate pH of 2 by addition of ultrapure 6 M HCl.

During the GA02 section (cruise PE321), additional seawater for dissolved ( $< 0.2 \mu\text{m}$ ) multi-element trace metal analysis was collected with an all-titanium ultraclean CTD sampling system metals<sup>61</sup> using samplers constructed from polyvinylidene difluoride (PVDF)<sup>62</sup>. Samples were filtered from the PVDF samplers under pressure (1.5 atm) from inline pre-filtered nitrogen gas in a clean environment aboard the ship. The filters utilized were  $0.2 \mu\text{m}$  Sartobran-300 (Sartorius) filter cartridges. Samples were collected into pre-cleaned<sup>63</sup> LDPE sample bottles (500 ml), following five rinses of the bottles with the sampled seawater. Finally, filtered samples were acidified on board to a pH of 1.7 to 1.8 by addition of ultrapure HCl (Baseline, Seastar Chemicals).

Samples for particulate ( $> 0.45 \mu\text{m}$ ) elemental concentration analysis were collected during the GA06 section (cruise D361). In a clean environment, particles were collected directly from trace metal clean 101 OTE (Ocean Test Equipment) sample bottles, under pressure (1.7 bar) of filtered nitrogen gas, onto acid-cleaned 25 mm Supor polyethersulfone (PES) membrane disc filters (Pall,  $0.45 \mu\text{m}$ ). Samples were stored frozen ( $-20 \text{ }^\circ\text{C}$ ) until shore-based analysis.

The results reported here are limited to those obtained for only the shallowest filtered ( $< 0.2 \mu\text{m}$ ) and particulate ( $> 0.45 \mu\text{m}$ ) samples collected during the two respective cruises (9–25 m depth; Supplementary Table 1).

Eleven aerosol samples were collected for elemental and Pb isotope analysis on the GA06 section cruise in the eastern tropical North Atlantic (ETA) by high-volume sampling ( $1 \text{ m}^3 \text{ min}^{-1}$ ) onto Whatman 41 cellulose fibre filters ( $203 \text{ mm} \times 241 \text{ mm}$ )<sup>64,65</sup> (Supplementary Table 6). Sampling was automatically controlled according to the wind direction, and paused whenever the wind direction was unfavourable to avoid contamination from the ship’s emissions. The filters were cleaned before aerosol collection in acid baths of 0.5 M HCl (1 h) followed by 0.1 M  $\text{HNO}_3$  (1 h) with thorough rinses with 18.2 MΩ cm water from a Millipore system after removal from each acid bath, at the University of East Anglia. Filters were fitted into the sampling apparatus within a laminar flow hood. Three sampling blanks were collected during the cruise by placing clean filters into the sampling apparatus, without turning on the pumping system. In addition, one cleaned Whatman 41 filter was taken to assess the blank contribution from the filter material. Following sample collection, the filters were stored in zip-lock plastic bags and frozen at  $-20 \text{ }^\circ\text{C}$ .

**Seawater Pb concentration and isotope composition analysis.** The Pb concentrations and isotope compositions of the unfiltered seawater samples were determined using thermal ionization mass spectrometry (TIMS) following previously described analytical techniques<sup>66</sup> at Imperial College London. Briefly, Pb concentrations were determined on 50 ml of seawater by isotope dilution. Following equilibration with a known quantity of a Pb double spike ( $^{207}\text{Pb}$ – $^{204}\text{Pb}$ ), Pb was purified from the seawater by  $\text{Mg}(\text{OH})_2$  co-precipitation and a single-stage

ion exchange chromatography procedure, before analysis by TIMS. To distinguish measurements affected by spurious high blanks, Pb concentrations were measured in duplicate or triplicate for the majority of samples, and any anomalously high values were discarded. Measurements of Pb isotope compositions were conducted on Pb purified from about 2 l of seawater by Mg(OH)<sub>2</sub> co-precipitation and a two stage ion exchange chromatography procedure. Instrumental mass bias encountered during the TIMS analyses was corrected using a Pb double spike (<sup>207</sup>Pb–<sup>204</sup>Pb). Uncertainty in Pb concentrations (1 s.d.) and isotope compositions (2 s.d.) are assessed through replicate analyses of in-house seawater standards<sup>66</sup>.

The 0.2 μm filtered samples from the WTA were analysed for multiple metals, including Pb as described by Middag *et al.*<sup>67</sup>, at the University of California, Santa Cruz. Briefly, Nobias PA1 chelating resin was used to pre-concentrate the metals in the seawater sample and to remove interfering sea salts, before analysis on a sector-field inductively coupled plasma mass spectrometer (Thermo Element XR Magnetic Sector ICP-MS). Analyses of SAFe and GEOTRACES reference samples agreed with consensus values for Pb and results from a crossover station agreed between the different occupations<sup>67</sup>.

Determination of Pb in the particulate samples was carried out at the University of Plymouth using a three-step sequential acid digestion following the method of Ohnemus *et al.*<sup>68</sup>. All samples were analysed using ICP-MS (Thermo Fisher X Series 2) with use of a collision/reaction cell utilizing 7% H in He. Replicate blank filters were processed in the same manner and the mean value deduced from the samples. Evaluation of the digestion efficiency was assessed using certified reference materials (CRMs) BCR-414 (Trace elements in plankton; Institute for Reference Materials and Measurements) and SO-2 (podzolic B horizon soil; Canadian CRM Project) and the subsequent Pb data was in agreement with the certified values.

**Aerosol elemental and isotopic analysis.** Aerosol sample preparation was conducted within clean room laboratories at Imperial College London. A portion of each Whatman 41 filter (equivalent to ~25–50% of the total exposed filter area) was subjected to a 'total' digestion procedure with the aim of liberating all available Pb and Al for analysis. In addition, a second portion of each filter (equivalent to ~12–50% of the total exposed filter area) was subjected to leaching, with the aim of liberating the Pb and Al that is readily soluble in 'natural' waters for analysis, following previously published methods<sup>54,64,65</sup>. The filter portions were taken by cutting the filters using ceramic scissors into pieces that were collected in 60 ml or 90 ml Teflon vials inside a laminar flow bench.

For the total digestions, the Whatman 41 cellulose filter and organic material in the aerosol, were first treated on a hotplate in open fluoropolymer (Savillex) vials using, 10–20 ml 15.6 M HNO<sub>3</sub> at 90–120 °C, for 12–15 h; 10 ml 15.6 M HNO<sub>3</sub> + 1 ml 9.8 M H<sub>2</sub>O<sub>2</sub> at 90–120 °C, for 12–15 h; and 4 ml 15.6 M HNO<sub>3</sub> + 1 ml 11.6 M HClO<sub>4</sub>, starting at 120 °C and increasing to 220 °C over 12–15 h. Residual HClO<sub>4</sub> was removed by repeated cycles of refluxing with 1–2 ml 15.6 M HNO<sub>3</sub> and evaporation to dryness at 140–220 °C. During the third step, 1–2 ml of 15.6 M HNO<sub>3</sub> was added periodically to dilute the HClO<sub>4</sub> and help control the rate of the reaction. The second step was omitted for filter portions representing <50% of the total exposed area and the third step was repeated if the digestion of organics was incomplete. Following this, the aerosol samples were digested in closed vials in 3 ml 15.6 M HNO<sub>3</sub> + 1 ml 28 M HF, at 120–140 °C for 4 days, with regular treatment in an ultrasonic bath. Finally, the HNO<sub>3</sub>–HF solutions were evaporated to dryness and samples were re-dissolved in 4 M HNO<sub>3</sub>. The Pb blank of the total digestion procedure was 53 ± 48 pg (1 s.d., *n* = 7), which is <0.05% of the sample Pb and therefore negligible.

For the leaching of filters, Whatman 41 filter portions were submerged in an ammonium acetate solution (~0.5 M aqueous NH<sub>3</sub> solution–1 M acetic acid, pH 4.7; 25 ml of solution per 25% of total exposed filter area) and shaken for 60 min at 200 r.p.m. The solutions were then passed through 0.2 μm Whatman cellulose acetate filters within 60–75 min of the addition of the leaching solutions. The filtered solutions were evaporated to dryness and re-dissolved in 4 M HNO<sub>3</sub>. The Pb blank of the leaching procedure was 48 ± 27 pg (1 s.d., *n* = 6), which is <0.05% of the liberated Pb in the samples and is therefore negligible.

Elemental concentrations (Pb and Al) were determined on 10% aliquots of the total digestion and leach solutions, which were evaporated to dryness and re-dissolved a suitable volume of 1 M HNO<sub>3</sub>. Lead concentrations (average of <sup>206</sup>Pb, <sup>207</sup>Pb and <sup>208</sup>Pb) were determined using an Agilent 7700x quadrupole ICP-MS instrument in the 'no gas' mode of the collision-reaction cell, at the Natural History Museum, London. Aluminium concentrations were determined for the total digestion solutions by inductively coupled plasma atomic emission spectroscopy (ICP-AES) using a Thermo iCap 6500 Duo instrument, also at the Natural History Museum, London. For the leach solutions, Al concentrations were determined by quadrupole ICP-MS.

The Pb blank content of the aerosol sampling and digestion/leaching methods were determined using 'blank' Whatman 41 filters to be 25 ± 16 ng filter<sup>-1</sup> (1 s.d., *n* = 4) for the total digestion procedure, and 12 ± 7 ng filter<sup>-1</sup> (1 s.d., *n* = 4) for the leaching technique. Since these blanks correspond to contributions of between 0.4 and 7.2% of the Pb extracted by the total digestion and leach procedures, the Pb concentrations were corrected for this blank using the mean values. Atmospheric Pb and Al concentrations were calculated from the determined concentrations and the known volume of the air sampled (Supplementary Table 6). The uncertainty of the atmospheric Pb concentrations

was calculated by propagating the 1 s.d. of the mean blank values though the blank correction.

Lead isotope compositions were determined on aliquots (0.6–53%) of the total digestion and leach solutions, corresponding to 10–100 ng of Pb (typically 20 ng Pb), at Imperial College London. Lead was purified from the sample matrix by processing through a two-stage ion exchange chromatography procedure adapted from Paul *et al.*<sup>66</sup> (Supplementary Table 7). The blank contribution of the ion exchange procedure was 14 ± 13 pg (2 s.d., *n* = 7), which is <0.3% of the Pb processed and is therefore negligible. The isotope composition of the purified Pb was subsequently analysed using the same measurement protocols as for seawater samples<sup>66</sup>.

Loads of 10 and 20 ng SRM NIST 981 Pb (common Pb isotopic standard) were analysed at the start of every measurement session, with values in good agreement with literature results (Supplementary Table 8). The basaltic reference materials BCR-2 and BHVO-2 (US Geological Survey), with about 20 ng of Pb, were also processed through the ion exchange procedure and analysed alongside the samples. To this end, powdered aliquots of 0.04–0.2 g of these reference materials were digested in a 3:1 mixtures of 28 M HF and 15.6 M HNO<sub>3</sub> (total volume of 6–8 ml), at 140 °C for 4 days with regular treatments in an ultrasonic bath, before chemical separation. Results are in good agreement with published reference values (Supplementary Table 8). The reproducibility of the <sup>206</sup>Pb/<sup>204</sup>Pb, <sup>206</sup>Pb/<sup>207</sup>Pb and <sup>208</sup>Pb/<sup>207</sup>Pb ratios of BCR-2 (*n* = 9) are taken to be representative for the samples.

The blank of the Whatman 41 filters and the sampling procedure contributes significantly to the total amount of Pb in the aerosol samples (0.4–7.2%). The Pb isotope data of the aerosols were hence corrected of this blank contribution, using the mean Pb contents and isotope compositions determined for the blank filters. The isotope composition determined for the blank filters subjected to the total digestion procedure was <sup>206</sup>Pb/<sup>204</sup>Pb = 18.40 ± 0.61, <sup>206</sup>Pb/<sup>207</sup>Pb = 1.175 ± 0.037 and <sup>208</sup>Pb/<sup>207</sup>Pb = 2.437 ± 0.023 (mean ± 2 s.d., *n* = 4). For the leaching procedure blank, the respective results were 18.32 ± 0.30, 1.172 ± 0.022 and 2.437 ± 0.012 (mean ± 2 s.d., *n* = 4).

The uncertainty of the blank correction was calculated by separately propagating through the blank correction (1) the 1 s.d. uncertainty of the mean blank content (the larger 2 s.d. uncertainty yields unrealistic negative values), and (2) the 2 s.d. of the blank isotope composition. The total uncertainty for each sample was then calculated by standard addition of variances from (1) the propagated uncertainty in the blank contribution (1 s.d.), (2) the propagated uncertainty of the blank isotope compositions (2 s.d.), and (3) the 2 s.d. reproducibility of the replicate Pb isotope analyses of 20 ng BCR-2 aliquots. The former two variances encompass the uncertainty generated by the Pb blank encountered during sample collection, while the latter variance accounts for the uncertainty induced by the chemical separation and mass spectrometric analysis.

**Data availability.** All relevant data are either presented in the main article or Supplementary Information File and are available from the authors at request.

## References

- Nriagu, J. O. & Pacyna, J. M. Quantitative assessment of worldwide contamination of air, water and soils by trace-metals. *Nature* **333**, 134–139 (1988).
- Boyle, E. A. *et al.* Anthropogenic lead emission in the ocean the evolving global experiment. *Oceanography* **27**, 69–75 <http://dx.doi.org/10.5670/pceanog.2014.10> (2014).
- Reuer, M. K. & Weiss, D. J. Anthropogenic lead dynamics in the terrestrial and marine environment. *Philos. Trans. A Math. Phys. Eng. Sci.* **360**, 2889–2904 (2002).
- Pacyna, J. M. & Pacyna, E. G. An assessment of global and regional emissions of trace metals to the atmosphere from anthropogenic sources worldwide. *Environ. Rev.* **9**, 296–298 (2001).
- Veron, A. J., Church, T. M., Flegal, A. R., Patterson, C. C. & Erel, Y. Response of lead cycling in the surface sargasso sea to changes in tropospheric input. *J. Geophys. Res. Oceans* **98**, 18269–18276 (1993).
- Wu, J. F. & Boyle, E. A. Lead in the western North Atlantic Ocean: completed response to leaded gasoline phaseout. *Geochim. Cosmochim. Acta* **61**, 3279–3283 (1997).
- Kelly, A. E., Reuer, M. K., Goodkin, N. F. & Boyle, E. A. Lead concentrations and isotopes in corals and water near Bermuda, 1780–2000. *Earth Planet. Sci. Lett.* **283**, 93–100 (2009).
- Veron, A. J., Church, T. M., Patterson, C. C. & Flegal, A. R. Use of stable lead isotopes to characterize the sources of anthropogenic lead in North-Atlantic surface waters. *Geochim. Cosmochim. Acta* **58**, 3199–3206 (1994).
- Alleman, L. Y. *et al.* Isotopic evidence of contaminant lead in the South Atlantic troposphere and surface waters. *Deep-Sea Res. Pt. II* **48**, 2811–2827 (2001).
- Weiss, D. *et al.* Spatial and temporal evolution of lead isotope ratios in the North Atlantic Ocean between 1981 and 1989. *J. Geophys. Res. Oceans* **108** (2003).

11. Noble, A. E. *et al.* Dynamic variability of dissolved Pb and Pb isotope composition from the U.S. North Atlantic GEOTRACES transect. *Deep-Sea Res. Pt. II* **116**, 208–225 (2015).
12. Boyle, E. A., Chapnick, S. D. & Shen, G. T. Temporal variability of lead in the western North Atlantic. *J. Geophys. Res.* **91**, 8573–8593 (1986).
13. Bacon, M. P., Spencer, D. W. & Brewer, P. G.  $^{210}\text{Pb}$ ,  $^{226}\text{Ra}$  and  $^{210}\text{Po}$ - $^{210}\text{Pb}$  disequilibria in seawater and suspended particulate matter. *Earth Planet. Sci. Lett.* **32**, 277–296 (1976).
14. Rigaud, S., Stewart, G., Baskaran, M., Marsan, D. & Church, T.  $^{210}\text{Po}$  and  $^{210}\text{Pb}$  distribution, dissolved-particulate exchange rates, and particulate export along the North Atlantic US GEOTRACES GA03 section. *Deep-Sea Res. Pt. II* **116**, 60–78 (2015).
15. Goudie, A. S. & Middleton, N. J. Saharan dust storms: nature and consequences. *Earth. Sci. Rev.* **56**, 179–204 (2001).
16. United Nations Environmental Program. <http://www.unep.org/Transport/new/PCFV/accessed2016>.
17. Ben-Ami, Y., Koren, I., Altartaz, O., Kostinski, A. & Lehahn, Y. Discernible rhythm in the spatio/temporal distributions of transatlantic dust. *Atmos. Chem. Phys.* **12**, 2253–2262 (2012).
18. Prospero, J. M., Collard, F. X., Molinie, J. & Jeannot, A. Characterizing the annual cycle of African dust transport to the Caribbean Basin and South America and its impact on the environment and air quality. *Global Biogeochem. Cycles* **28**, 757–773 (2014).
19. Chiapello, I. *et al.* An additional low layer transport of Sahelian and Saharan dust over the North-Eastern Tropical Atlantic. *Geophys. Res. Lett.* **22**, 3191–3194 (1995).
20. Patey, M. D., Achterberg, E. P., Rijkenberg, M. J. & Pearce, R. Aerosol time-series measurements over the tropical Northeast Atlantic Ocean: Dust sources, elemental compositions and mineralogy. *Mar. Chem.* **174**, 103–119 (2015).
21. Adams, A. M., Prospero, J. M. & Zhang, C. CALIPSO-derived three-dimensional structure of aerosol over the Atlantic basin and adjacent continents. *J. Clim.* **25**, 6862–6879. <http://dx.doi.org/10.1175/JCLI-D-11-00672.1> (2012).
22. Powell, C. F. *et al.* Estimation of the atmospheric flux of nutrients and trace metals to the eastern tropical North Atlantic Ocean. *J. Atmos. Sci.* **72**, 4029–4045 (2015).
23. Bollhofer, A. & Rosman, K. J. R. Isotopic source signatures for atmospheric lead: The Northern Hemisphere. *Geochim. Cosmochim. Acta* **65**, 1727–1740 (2001).
24. Witt, M., Baker, A. R. & Jickells, T. D. Atmospheric trace metals over the Atlantic and South Indian Oceans: Investigation of metal concentrations and lead isotope ratios in coastal and remote marine aerosols. *Atmos. Environ.* **40**, 5435–5451 (2006).
25. Kumar, A. *et al.* A radiogenic isotope tracer study of transatlantic dust transport from Africa to the Caribbean. *Atmos. Environ.* **82**, 130–143 (2014).
26. Abouchami, W. & Zabel, M. Climate forcing of the Pb isotope record of terrigenous input into the Equatorial Atlantic. *Earth Planet. Sci. Lett.* **213**, 221–234 (2003).
27. Chow, T. J. & Patterson, C. C. The occurrence and significance of lead isotopes in pelagic sediments. *Geochim. Cosmochim. Acta* **26**, 263–308 (1962).
28. Abouchami, W. *et al.* Geochemical and isotopic characterization of the Bodele Depression dust source and implications for transatlantic dust transport to the Amazon Basin. *Earth Planet. Sci. Lett.* **380**, 112–123 (2013).
29. Allègre, C. J., Dupré, B., Nègre, P. & Gaillardet, J. Sr-Nd-Pb isotope systematics in Amazon and Congo River systems: constraints about erosion processes. *Chem. Geol.* **131**, 93–112 (1996).
30. Asmerom, Y. & Jacobsen, S. B. The Pb isotopic evolution of the Earth: inferences from river water suspended loads. *Earth Planet. Sci. Lett.* **115**, 245–256 (1993).
31. Rijkenberg, M. J. A. *et al.* The distribution of dissolved iron in the West Atlantic Ocean. *PLoS ONE* **9** <http://dx.doi.org/10.1371/journal.pone.0101323> (2014).
32. Dulaquais, G. *et al.* Contrasting biogeochemical cycles of cobalt in the surface western Atlantic Ocean. *Global Biogeochem. Cycles* **28**, 1387–1412 (2014).
33. Steding, D. J., Dunlap, C. E. & Flegal, A. R. New isotopic evidence for chronic lead contamination in the San Francisco Bay estuary system: implications for the persistence of past industrial lead emissions in the biosphere. *Proc. Natl Acad. Sci. USA* **97**, 11181–11186 (2000).
34. Raes, F. *et al.* Formation and cycling of aerosols in the global troposphere. *Atmos. Environ.* **34**, 4215–4240 (2000).
35. Draxler, R. R. & Rolph, G. D. *HYSPLIT (Hybrid Single-Particle Lagrangian Integrated Trajectory) Model access via NOAA*. ARL. <http://www.arl.noaa.gov/ready/hysplit4.html> (NOAA Air Resources Laboratory, Silver Spring, MD, 2003); <http://www.arl.noaa.gov/ready/hysplit4.html>.
36. Guerzoni, S. *et al.* Role of desert aerosol in metal fluxes in the Mediterranean area. *Chemosphere* **39**, 229–246 (1999).
37. Kersten, M., Kriews, M. & Forstner, U. Partitioning of trace-metals released from polluted marine aerosols in coastal seawater. *Mar. Chem.* **36**, 165–182 (1991).
38. Chester, R. *et al.* Factors controlling the solubilities of trace-metals from nonremote aerosols deposited to the sea-surface by the dry deposition mode. *Mar. Chem.* **42**, 107–126 (1993).
39. Hsu, S. C., Lin, F. J. & Jeng, W. L. Seawater solubility of natural and anthropogenic metals within ambient aerosols collected from Taiwan coastal sites. *Atmos. Environ.* **39**, 3989–4001 (2005).
40. Maring, H. B. & Duce, R. A. The impact of atmospheric aerosols on trace-metal chemistry in open ocean surface seawater 3 lead. *J. Geophys. Res. Oceans* **95**, 5341–5347 (1990).
41. Spokes, L. J., Jickells, T. D. & Lim, B. Solubilization of aerosol trace-metals by cloud processing—a laboratory study. *Geochim. Cosmochim. Acta* **58**, 3281–3287 (1994).
42. Desboeufs, K. V., Sofikitis, A., Losno, R., Colin, J. L. & Ausset, P. Dissolution and solubility of trace metals from natural and anthropogenic aerosol particulate matter. *Chemosphere* **58**, 195–203 (2005).
43. Chester, R. *et al.* Defining the chemical character of aerosols from the atmosphere of the Mediterranean-Sea and surrounding regions. *Oceanol. Acta* **16**, 231–246 (1993).
44. Chester, R., Saydam, A. C. & Sharples, E. J. An approach to the assessment of local trace-metal pollution in the Mediterranean marine atmosphere. *Mar. Pollut. Bull.* **12**, 426–431 (1981).
45. Gelado-Caballero, M. D. *et al.* Long-term aerosol measurements in Gran Canaria, Canary Islands: Particle concentration, sources and elemental composition. *J. Geophys. Res. Atmos.* **117**, doi:10.1029/2011JD016646 (2012).
46. Rudnick, R. & Gao, S. Composition of the continental crust. *Treatise Geochem.* **3**, 1–64 (2003).
47. Mackey, K. R. M., Chien, C. T., Post, A. F., Saito, M. A. & Paytan, A. Rapid and gradual modes of aerosol trace metal dissolution in seawater. *Front. Microbiol.* **5**, doi:10.3389/fmicb.2014.00794 (2015).
48. Flegal, A. R., Maring, H. & Niemeier, S. Anthropogenic lead in Antarctic seawater. *Nature* **365**, 242–244 (1993).
49. Nriagu, J. O. The rise and fall of leaded gasoline. *Sci. Total Environ.* **92**, 13–28 (1990).
50. TERNON, E. *et al.* The impact of Saharan dust on the particulate export in the water column of the North Western Mediterranean Sea. *Biogeosciences* **7**, 809–826 (2010).
51. Arimoto, R., Ray, B. J., Lewis, N. F., Tomza, U. & Duce, R. A. Mass-particle size distributions of atmospheric dust and the dry deposition of dust to the remote ocean. *J. Geophys. Res. Atmos.* **102**, 15867–15874 (1997).
52. Fomba, K. A., Muller, K., van Pinxteren, D. & Herrmann, H. Aerosol size-resolved trace metal composition in remote northern tropical Atlantic marine environment: case study Cape Verde Islands. *Atmos. Chem. Phys. Discuss.* **12**, 29535–29569 (2012).
53. Duce, R. A. *et al.* The atmospheric input of trace species to the world ocean. *Global Biogeochem. Cycles* **5**, 193–259 (1991).
54. Baker, A. R., Adams, C., Bell, T. G., Jickells, T. D. & Ganzeveld, L. Estimation of atmospheric nutrient inputs to the Atlantic Ocean from 50°N to 50°S based on large-scale field sampling: iron and other dust-associated elements. *Global Biogeochem. Cycles* **27**, 755–767 (2013).
55. Chester, R., Nimmo, M. & Preston, M. R. The trace metal chemistry of atmospheric dry deposition samples collected at Cap Ferrat: a coastal site in the Western Mediterranean. *Mar. Chem.* **68**, 15–30 (1999).
56. Kidd, C. & Huffman, G. Global precipitation measurement. *Meteorol. Appl.* **18**, 334–353 (2011).
57. Helmers, E. & Schrems, O. Wet deposition of metals to the tropical north and the south-Atlantic Ocean. *Atmos. Environ.* **29**, 2475–2484 (1995).
58. Schlosser, C. *et al.* Seasonal ITCZ migration dynamically controls the location of the (sub)tropical Atlantic biogeochemical divide. *Proc. Natl Acad. Sci. USA* **111**, 1438–1442 (2014).
59. Middag et al. Dissolved aluminium in the ocean conveyor of the West Atlantic Ocean: effects of the biological cycle, scavenging, sediment resuspension and hydrography. *Mar. Chem.* **177**, 69–86 (2015).
60. Huneus, N. *et al.* Global dust model intercomparison in aerocom phase I. *Atmos. Chem. Phys.* **11**, 7781–7816 (2011).
61. De Baar, H. J. W. *et al.* Titan: a new facility for ultraclean sampling of trace elements and isotopes in the deep oceans in the international Geotraces program. *Mar. Chem.* **111**, 4–21 (2008).
62. Rijkenberg, M. J. A. *et al.* 'PRISTINE', a new high volume sampler for ultraclean sampling of trace metals and isotopes. *Mar. Chem.* **117**, 501–509 (2015).
63. Middag, R., de Baar, H. J. W., Laan, P. & Bakker, K. Dissolved aluminium and the silicon cycle in the Arctic Ocean. *Mar. Chem.* **115**, 176–195 (2009).

64. Sarthou, G. *et al.* Atmospheric iron deposition and sea-surface dissolved iron concentrations in the eastern Atlantic Ocean. *Deep-Sea Res. Pt. I* **50**, 1339–1352 (2003).
65. Baker, A. R., French, M. & Linge, K. L. Trends in aerosol nutrient solubility along a west-east transect of the Saharan dust plume. *Geophys. Res. Lett.* **33**, doi:10.3389/fmicb.2014.00794 (2006).
66. Paul, M., Bridgestock, L., Rehkamper, M., van de Flierdt, T. & Weiss, D. High-precision measurements of seawater Pb isotope compositions by double spike thermal ionization mass spectrometry. *Anal. Chim. Acta.* **863**, 59–69 (2015).
67. Middag, R. *et al.* Intercomparison of dissolved trace elements at the Bermuda Atlantic Time Series station. *Mar. Chem.* **117**, 476–489 (2015).
68. Ohnemus, D. C. *et al.* Laboratory intercomparison of marine particulate digestions including Piranha: a novel chemical method for dissolution of polyethersulfone filters. *Limnol. Oceanogr. Methods* **12**, 530–547 (2014).
69. Schlitzer, R. Interactive analysis and visualization of geoscience data with Ocean Data View. *Comput. Geosci.* **28**, 1211–1218 (2002).
70. Acker, J. G. & Leptoukh, G. Online Analysis Enhances Use of NASA Earth Science Data. In *Paper presented at the Eos, Transactions American Geophysical Union.* giovanni.gsfc.nasa.gov/giovanni/ (2007).

### Acknowledgements

We thank the captain, crew and cruise participants of the *RRS Discovery* during the D361 cruise (GEOTRACES section GA06), and of the *RV Pelagia* during the 64PE321 cruise (GEOTRACES section GA02, 2nd leg). Gideon Henderson and Stephen Galer are thanked for providing useful comments on the work. Katharina Kreissig and Barry Coles kept the MAGIC clean labs and mass spectrometer running, while the MAGIC research group provided their support and guidance. The authors acknowledge funding from the following NERC grants: L.B., T. v.d.F. and M.R. by NE/J021636/1 and NE/H005390/1; R.C. and A.B. by NE/G016585/1; E.P.A. and M.L. by NE/G015732/1.

### Author contributions

L.B., T.v.d. F. and M.R. conceived the study, and L.B. conducted all Pb concentration and isotope analyses of unfiltered seawater and aerosol samples with assistance from M.P.

Lead concentration measurements of filtered seawater were conducted by R.M, and by A.M and M.C.L. for particulate samples. Digestion and leaching of the aerosols was conducted by L.B with assistance from R.K. Determination of the Pb and Al concentrations of the aerosol samples was conducted by S.S and E.H.W. Credit for sample collection goes to M.C.L and E.P.A for the GA06 section, while A.R.B and R.C are specifically credited with collection of the aerosol samples. For the GA02 section, sample collection is credited to M.J.A.R and L.J.A.G. The initiative and programme proposal for the GA02 section, which was partly covered by cruise 64PE321, was by H.J.W.de B jointly with M.J.A.R and L.J.A.G. The manuscript was written by L.B with inputs received from all co-authors.

### Additional information

**Supplementary Information** accompanies this paper at <http://www.nature.com/naturecommunications>

**Competing financial interests:** The authors declare no competing financial interests.

**Reprints and permission** information is available online at <http://npg.nature.com/reprintsandpermissions/>

**How to cite this article:** Bridgestock, L. *et al.* Return of naturally sourced Pb to Atlantic surface waters. *Nat. Commun.* **7**, 12921 doi: 10.1038/ncomms12921 (2016).



This work is licensed under a Creative Commons Attribution 4.0 International License. The images or other third party material in this article are included in the article's Creative Commons license, unless indicated otherwise in the credit line; if the material is not included under the Creative Commons license, users will need to obtain permission from the license holder to reproduce the material. To view a copy of this license, visit <http://creativecommons.org/licenses/by/4.0/>

© The Author(s) 2016